J. Synchrotron Rad. (1997). **4**, 67–77

Calibration and Application of an X-ray Image Intensifier/ Charge-Coupled Device Detector for Monochromatic Macromolecular Crystallography

A. P. Hammersley,[a] K. Brown,[b] W. Burmeister,[a] L. Claustre,[b] A. Gonzalez,[a]† S. McSweeney,[b] E. Mitchell,[a] J.-P. Moy,[a]‡ S. O. Svensson[a] and A. W. Thompson[b]

[a]ESRF, BP 220, 38043 Grenoble, France, and [b]EMBL Outstation, BP 156, 38042 Grenoble, France. E-mail: hammersley@esrf.fr

(*Received 9 July 1996; accepted 3 December 1996*)

Charge-coupled device (CCD)-based X-ray detectors allow data to be collected much more quickly (~10 times) than with current on-line imaging-plate systems. At the ESRF, X-ray image intensifier/CCD detector systems have been developed. These have great potential as fast read-out detectors for macromolecular and other forms of crystallography. They are relatively large sensitive X-ray detectors but have two inherent weaknesses: convex detection surfaces leading to spatial distortion and non-uniformity of intensity response, and susceptibility to small changes in magnetic fields. A large improvement has been made to the accuracy obtained by non-uniformity of response calibration and correction, using fluorescence from doped lithium borate glasses. Monochromatic macromolecular crystallography demonstration experiments with external user groups have shown that high-quality results may be obtained under real experimental conditions.

Keywords: detector calibration; data collection; detector distortions; X-ray detectors; charge-coupled device detectors; macromolecular crystallography.

1. Introduction

X-ray detector systems using charge-coupled devices (CCDs) are presently attracting a large amount of interest for crystallographic measurements, especially at synchrotron radiation sources. CCDs are solid-state electronic integrated circuits suitable for fast read-out. The fast read-out means that the systems may be used on-line with much less 'dead time' owing to read-out than with imaging-plate-based detectors.

Generally, a conversion stage is used to convert the X-rays to visible light which is detected by the CCD. As CCDs have a smaller surface area than the required X-ray detection area, a demagnification stage must also be introduced. One detector design which is presently being used consists of a phosphor to convert the X-rays to visible photons, followed by a fibre-optic taper to demagnify the image from the phosphor onto a smaller CCD (Naday *et al.*, 1995; Tate *et al.*, 1995). Installed at the Cornell High Energy Synchrotron Source (CHESS), several systems of the same basic design are being used successfully for macromolecular crystallography (Naday, Ross, Kanyo, Westbrook & Westbrook, 1994; Thiel *et al.*, 1995; Walter *et al.*, 1995). The input size of the detector is severely limited by the screen–CCD coupling efficiency which decreases with the square of the demagnification, with lenses as well as with fibre-optic tapers. Fibre-optic tapers are more efficient than lenses for demagnification (Deckman & Gruner, 1986), but become increasingly difficult to manufacture when their size exceeds 50–80 mm.

An alternative approach to overcome this basic limitation is to use an X-ray image intensifier (XRII) to produce a demagnified and amplified visible-light image which can be relayed onto a CCD by a lens system (see Fig. 1). The ESRF Detector Group have developed a modular system of X-ray detectors using specially commissioned beryllium entrance-window intensifiers and also standard aluminium-window medical XRIIs optically coupled to a variety of CCD cameras (Moy, 1994).

The beryllium-windowed XRII allows good detective quantum efficiency down to 5 keV. With the gain of the XRII being very large, the overall conversion factor of the system is easily adjusted by stopping down the lens without adding extra noise. For a wide range of X-ray energies and fluxes, the gain can be adjusted so that each incoming X-ray contributes as many electrons in the CCD as the total noise of the dark count and read-out noise. For special applications the gain can be adjusted such that each X-ray produces many more electrons than the system noise; however, this reduces the dynamic range of the system. Given the high transparency of the beryllium window and the high absorption of the CsI detection layer, for fluxes

† Present address: EMBL Outstation, c/o DESY, Notkestrasse 85, 22603 Hamburg, Germany.

‡ Present address: Thomson Tubes Electroniques, ZI Centr'Alp, 38430 Moirans, France.

of more than a few X-rays per pixel the detective quantum efficiency is better than 50% between 6 and 25 keV.

The aluminium-windowed XRII is designed for medical X-rays so that its best performance is obtained at ~40–70 keV. However, it offers acceptable detective quantum efficiency (> 20%, given the above conditions) from 20 up to and beyond 100 keV.

As on-line fast read-out systems, the XRIIs have relatively large active surface areas; the beryllium-window XRII has an active diameter of 230 mm, and the aluminium-window XRII has an active diameter of 320 mm.

In general, CCD systems are a trade-off between dynamic range and read-out speed, and between the number of pixels, and both cost and dynamic range. It is advantageous to be able to choose one of a variety of different characteristic XRIIs (beryllium or aluminium, 'fast' phosphors or 'normal' higher resolution output phosphors) together with a large range of CCD devices. This is made possible by the modularity of the system and the easy exchange owing to the lens system. The characteristics of the 'detector system' may be customized to fit the required scientific application. For the present work, two different commercially available CCD systems were used together with a beryllium-window XRII with the standard P20 output phosphor:

(i) EEV 1242 × 1152 pixels controlled by a Princeton Instruments ST-138 controller. This has a 16-bit analog-to-digital converter (ADC) and a measured dynamic range greater than 15 bits.† The read-out speed may be 50, 100 or 150 kHz. At 150 kHz the full image can be read out in 9 s. This has been relayed to the output phosphor of the XRII by a Rodenstock Heliflex F/1.8 lens with a 112 mm focal length, and a Kinoptik F/2.5 apochromatic lens with a 150 mm focal length.

(ii) Tektronix 1024 × 1024 pixels controlled by a Photometrics AT200 controller. This has a 14-bit ADC and a measured dynamic range of 14 bits.† The read-out speed is 200 kHz, so a full image can be read out in 5 s. This system has a lower dark current owing to the multiphase pinned (MPP) circuitry. This was also relayed using the same Rodenstock lens but with a Schneider Cinexenon F/2 lens with a 130 mm focal length.

Both have a built-in Peltier cooling unit to reduce the dark noise of the CCD to a negligible value for exposures up to ~100 s (typical operating temperature is 223 K).

Other much faster read-out systems are also possible. At the ESRF, a fast read-out system has been developed, with 1024 × 1024 pixels and 14 bit dynamic range, which can be read out at 5 MHz (Labiche, Segura-Puchades, van Brussel & Moy, 1996). With one read-out channel this system can be read out in 0.2 s. However, the CCD system has four read-out channels available and so can be read out up to 20 times a second using four parallel read-out circuits into a VXI bus system. More-reduced dynamic range systems, typically 8 bits, exist at video frame speeds, and systems with much faster read-out speeds, up to hundreds of frames per second, are commercially available.

Whilst this type of X-ray detector has many advantages, it has two major disadvantages: an almost spherical detection surface curving away from the sample, and susceptibility to external magnetic fields. Spatial distortion and non-uniformity of intensity response in the recorded images are important problems and must be reliably corrected if these systems are to fulfil their potential.

One of the most challenging and important applications for these detectors is the field of X-ray crystallography, as both good positional and intensity accuracy are required. A program of development of calibration methods and test experiments has been realized using macromolecular crystallography samples. With suitable calibration, the test experiments showed that high-quality data may be collected. Finally, a series of demonstration scientific experiments with external groups were performed as the 'real test' of the system.

† The read-out noise has been measured at the three different standard read-out speeds and even at the fastest speed is 1.2 ADC units per pixel. At a 430 kHz read-out speed, which is available using an alternative ADC, the read-out noise is 1.8 ADC units per pixel. Simple linearity tests have shown the CCD to be reasonably linear until at least 60 000 ADC units.

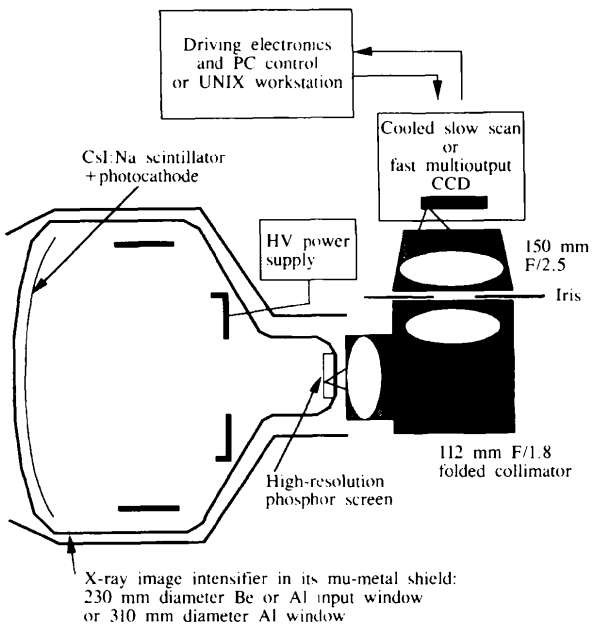

Figure 1
Diagram of the modular components of the X-ray image-intensifier/CCD detector system.

2. Detector distortions and calibration

2.1. *Magnetic shielding*

The problem of the convex detection surface may be considered as a problem of spatial distortion, or parallax, relative to a flat detector. Imperfections in the electron-focusing optics, external magnetic fields, and imperfections in the light optics can also lead to spatial distortions. Such detector distortions are not unique to XRIIs and various

† Read-out noise of less than 1 ADC unit per pixel with good linearity.

work with calibration and correction of distortions in other detectors exists (Thomas, 1989, 1990; Stanton, Philips, Li & Kalata, 1992).

Whilst methods exist to cope partially with continuous changes in distortions (Thomas, 1990), the necessary calibration and correction involved is much reduced if the distortions can be made to be sufficiently constant that calibration may be carried out separately from scientific experiments.

Following initial tests which showed some small but annoying drift in distortion with time, a system of Mu-metal shielding was added. The design was closely based on one made for the ESRF-based external beamline D2AM† (Fanchon, Ferrer, Kahn, Berthet & Roth, 1995). This magnetic shielding surrounds the intensifier and includes a choice of cones which extend the magnetic shielding in front of the entrance window towards the sample.

A series of tests showed that with the shielding the positional repeatability is of the order of 10–20 μm for a 12 h period. The removal and replacement of the front shielding cone was shown to also allow repeatability of ~20 μm. This is important as it is necessary to place a grid inside the cone for calibration, and this grid must be removed prior to collecting crystallographic data. As typical recorded peak sizes are approximately 500 μm across, this corresponds to a small enough fraction of the peak that profile fitting should work well. (It is estimated that the accuracy to which a peak centre is known needs to be ~1/15 of the peak size or better for profile fitting to work well.)

Whilst the shielding is desirable, it does cause potential collision problems for a diffractometer and may limit the sample-to-detector distance. The choice of cones, and the forward shielding being made of two pieces, allow reasonable flexibility. The distortion tests and experience with crystallographic samples showed that using one half of the forward shielding cone is sufficient for distortion drift not to be a problem.

2.2. *Spatial distortion correction*

The raw data may be impossible to index or will often be indexed wrongly if the spatial distortion is not first corrected or taken into account by the indexing software. Relative to the centre of the detector, and an average pixel size, the spatial distortion may be up to ~30 pixels towards the edge of the detector. As a typical peak may be four or five pixels across, this is more than enough to lead to indexing problems.

Our general approach to distortion calibration and correction is described by Hammersley, Svensson & Thompson (1994) and Hammersley *et al.* (1995). For calibration and characterization of the spatial distortion, a copper calibration grid mask was manufactured. This mask is made from a sandwich of two layers of 35 μm of copper on top of a fibre-glass support which is 150 μm thick. Copper was chosen for the mask material to avoid magnetic effects from the mask causing extra distortions. The thickness gives the mask very high contrast at 1.0 Å wavelength radiation and allows reasonable opaqueness up to ~0.6 Å. This material is normally used for mounting electronic components. An orthogonal grid of 400 μm diameter holes at a spacing of 5 mm was accurately drilled into the support.

For the tests and experiments to date we have always calibrated the detector *in situ*. This allows exactly the same parallax and absorption effects for spatial distortion and flat-field correction. The synchrotron X-ray beam has been used with a 'scattering' sample to produce the X-ray illumination for calibration.

As long as there are no sharp features in the illumination, such as powder rings, the grid mask may be exposed with a variety of samples that lead to a diffuse emission. However, the width of the volume of interaction of the direct X-ray beam and the sample should be as small as possible. This is to give as good definition of the calibration and correction as possible. Whilst not absolutely necessary, it has been most convenient to use the same fluorescent glass sample for illumination of the calibration grid as is used for flood-field calibration (this is described in the following section). These give a very smooth emission and allow the sample thickness to be a fraction of a millimetre: 400 μm in the case of the strontium-doped glass sample which was mainly used.

The grid-mask images are processed using *FIT2D* (Hammersley, 1995). A peak-search algorithm finds the centre of each peak by cross-correlation with an ideal peak-shape function, and knowledge of the grid pattern spacing is used to define the spatial distortion as a discrete function of two-dimensional position. Two-dimensional spline surfaces are 'roughly' fitted to the measured distortion values with a user-supplied value for the average r.m.s. discrepancy. This discrepancy is chosen so that the spline surfaces closely follow the overall form of the distortion, but do not fit too closely to individual positions, which have errors. The spline coefficients may be saved and later used to interpolate a continuous distortion function at all pixel positions. The distortion correction is calculated for each distorted pixel and the input intensity is rebinned to an ideal Cartesian detector raster (Hammersley *et al.*, 1994).

2.3. *Non-uniformity of response correction*

The non-uniformity of response correction is theoretically a much simpler correction than the spatial distortion correction: you divide your data by a normalized flat-field response; in practice it has proven to be much more difficult to calibrate accurately.

The non-uniformity of response is a function of both experimental geometry and of X-ray energy, so ideally the best calibration should be made in the same geometry and with the same, or at least similar, X-ray energy. We do not know of a perfect isotropic point source at arbitrary X-ray

† The Mu-metal shielding is manufactured by Soudupin, Montereau 77130, France.

energies. However, we have found that very smooth 'flood-field'† emission may be obtained at a wide variety of X-ray energies by using the fluorescence from doped dilithium tetraborate glasses (Moy *et al.*, 1996). These glasses are relatively easy to manufacture from raw materials provided that a few basic preparation rules are followed (Foust, 1995). The glass ingots may be machined using normal optical glass methods.

Whilst these fluorescent samples give close to isotropic emission, the accuracy with which we would like to calibrate the flat-field response (~1%) means that it is necessary to take into account the emission of the sample. Whilst this could be characterized using another two-dimensional detector, *e.g.* an image plate, our main effort has been in trying to obtain circularly symmetric emission (with respect to the X-ray beam), and to characterize the emission fully using a 2θ scan with a photon-counting detector (Hammersley *et al.*, 1995).

To obtain circular symmetry it is important that the sample geometry be axially symmetric. A flat glass plate is the easiest geometry as it does not need precise positioning, but it does need to be orthogonal to the beam. This is because self-absorption is the major cause of reduced emission at higher angles. A spherical or hemispherical sample may be another interesting geometry, especially for high 2θ angle calibration. This would require very accurate positional alignment, but would not need to be accurately orthogonal to the beam. At present we have only used the flat-plate geometry.

With the flat-plate fluorescent sample we have successfully and independently used three different methods to achieve the necessary orthogonality.

(i) Optical: use of the sample-alignment microscope to align the glass sample. One tilt can be determined by adjusting the sample so that it is parallel with a graticule. (Normally such alignment systems have graticules: if not, the orthogonal position will need to be marked from the spindle or by another method.) The other tilt may be set by rotating the φ axis until the view of the glass is as narrow as possible. If the alignment camera is not orthogonal to the beam, but at a known angle, the φ axis will then need to be rotated by this angle.

(ii) Laser reflection: an alignment laser can be shone down the collimation system and reflected off the glass. The tilt angles of the glass may be adjusted until the reflected beam returns down the collimation system.

(iii) Measurement at equal angles: the X-ray emission can be measured at equal 2θ angles and the orientation adjusted so that the measurements are equal. This is probably the most accurate method but also the most time-consuming. Thus, the other methods are preferable, at least for initial alignment.

In practice, we have found that any of these methods may be used and estimate that an orthogonality error of less than 1° is necessary for accurate calibration. The method used has depended on the available facilities on the different experimental set-ups which we have used.

By mounting the fluorescent glass on a goniostat head with a tilt cradle, the optimum tilt and diffractometer φ angle may be set and the goniostat removed from the experiment and stored. It may then be later re-used without the need for realignment.

FIT2D was used to process the 2θ-scan data and the flood-field images (Hammersley, 1995). The 2θ scan is normalized for beam decay, either by a simple linear interpolation of the synchrotron beam current at the start and end of the scan, or, when available, by dividing by a record of the main X-ray beam intensity. At the ESRF, the electron beam lifetime is such that the error due to the linear approximation is negligible.

Fig. 2 shows the normalized '2θ scan' measured from a strontium-doped sample excited using 16.1 keV X-rays, with fluorescence at 14.2 keV. The very high degree of symmetry of the scan suggests that the error in repeatability is of the order of 0.25%; however, it is the error in the full two-dimensional distribution which is important for this technique. (Note that the large dip in the centre of the scan is asymmetric due to the shadow of the beam-stop being slightly asymmetric with respect to the direct beam.) The degree of circular symmetry in the two-dimensional distribution is further considered by Moy *et al.* (1996).

The flood-field illumination may be corrected to a flat field by dividing by the normalized source emission as a function of angle (correcting for the effects of polarization, $1/r^2$ drop-off, obliqueness angle on the flat detector, and off-axis air absorption).

It should be emphasized that the order in which the various detector distortion corrections are applied is important, and that corrections need to be applied to the calibration data. One possible scheme has been suggested by Hammersley *et al.* (1995).

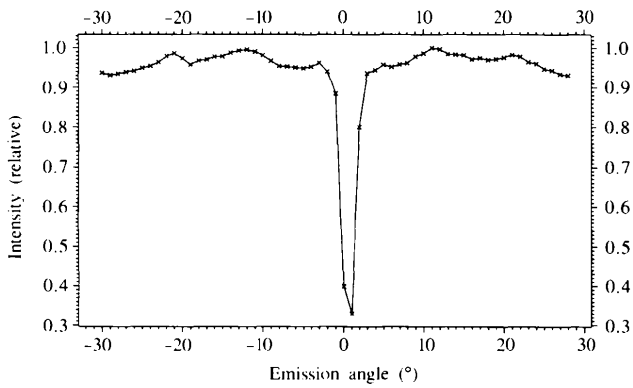

Figure 2
The normalized emission as a function of angle from a 400 μm wide strontium-doped dilithium tetraborate sample.

† We refer to an illumination which is smooth and continuous, but is neither totally uniform nor isotropic, as a 'flood-field'. An illumination which is totally uniform (planar), or isotropic from a point source, we refer to as a 'flat-field' illumination. In most crystallographic applications it is most useful to correct for the response from an isotropic point source.

3. Development of calibration methods and verification experiments

3.1. *Experimental set-up*

A series of test experiments were performed on ESRF beamline BM-5 to develop and refine calibration and data-collection methods. This resulted in improvements to the calibration process and also in the steady improvement of data quality obtained from test samples.

A silicon (111) monochromator was used; no focusing was available during these experiments. The monochromator crystals were detuned to provide harmonic rejection. A beam of $\sim 0.5 \times 0.5$ mm at the sample was selected using slits. The oscillation method was used with an Arndt–Wonacott camera, the total time and number of oscillations being varied according to the sample.

A beryllium-window XRII with a Photometrics CCD camera controlled by a PC was used to obtain integrated two-dimensional images of the diffraction patterns. The synchronization of the φ spindle oscillation range, the X-ray shutter and the CCD camera shutter was achieved using a hardware solution: the ESRF vct6 timer/counter VME card. An automated data-collection procedure was developed using a spec™ macro and a corresponding macro for the Photometrics CCD camera control software. The synchronization between the two systems was through TTL trigger lines and was tested using a laser, photodiode and a digital oscilloscope.

3.2. *Data calibration and correction*

Data-collection and calibration protocols were developed to ensure that all necessary calibration measurements were carried out at appropriate times. It is, for example, important to measure the distance from the calibration grid to the sample position when the grid is mounted, as this is the effective sample-to-detector distance for the spatially corrected data. If possible, it is preferable to carry out calibration prior to collection of crystallographic data, but when suitable sample-to-detector distances are unknown prior to initial sample exposures it may be necessary to perform the calibration measurements at the end of the experiment. For the test experiments, calibration was carried out both at the start and end of the experiments in order to verify the stability of the distortions. No significant drift was found, even when several days elapsed between calibration measurements, and this is now considered unnecessary for normal experiments.

During the early test experiments it was realized that R factors from integrated intensities produced by *DENZO* (Otwinowski, 1993) profile fitting were poorer than from the simple box integration. Various explanations for this were suggested, but it turned out to be correlated to strong exposures and was eventually attributed to saturated peaks affecting the profile-fitting method. In retrospect, the manner in which saturated peaks, which are not identified as such, adversely affect the profile fitting is easy to understand.

To avoid this problem it is necessary to preserve knowledge of the saturated peaks throughout the data processing. Here we consider each stage of the processing where a problem could occur.

The first stage of data processing is to subtract the detector offset values from each pixel. This operation in itself will bring pixel intensity values below the normal saturation value. Since the offset value is not identical for every pixel it is not sufficient simply to reduce the value of the saturation limit. Instead, prior to the subtraction, all saturated pixels are identified and a large intensity value is added to each pixel value. Thus, even after the subtraction of the offset values, these pixels are still well above the saturation value.

The next stage of processing where knowledge of the saturated pixels may be lost is the rebinning of the spatially distorted image to an ideal Cartesian raster. This may involve the distribution of the intensity of one input pixel into typically four output pixels, the distribution of intensity normally being in proportion to the covered area. In the case where the input pixel was saturated, this procedure was altered such that the input pixel value was added in its entirety to each of the partially covered output pixels. This operation clearly alters the integrated intensities, but since it is only of saturated peaks it does not affect the integration results and statistics. Whilst we did not try to use profile fitting to obtain estimated intensities from peaks containing saturated pixels, this would still be possible. However, the number of affected pixels will in general be greater than would be the case for the raw data.

The final stage of the preprocessing which may affect intensities is the flat-field correction. Since the non-uniformity of response varies by $\sim 40\%$ from the centre of the detector to the edge, and by $\sim 10\%$ azimuthally, pixel intensity values are corrected by varying amounts. However, if the truly saturated pixels have already had a value which is more than twice the detector saturation limit added to them, the correction can be arranged so that they are still above the limit.

In practice, the 'saturation' level can be set below the CCD saturation level, *e.g.* if high-end non-linearity is suspected.

3.3. *Results from test diffraction experiments*

The last test experiments were carried out on BM-5 in March 1995 using tetragonal hen-egg-white lysozyme crystals. The data were integrated using *DENZO*, and processing statistics from *AGROVATA* (Collaborative Computational Project, Number 4, 1994) are shown in Table 1. The data were both corrected for detector distortions and integrated whilst the experiment was being performed. Previous experiments had involved an iterative process of processing, understanding problems, and reprocessing data, prior to obtaining satisfactory results.

The processing statistics suggest that the data was of good quality and that all aspects of the experiment and analysis were correct. Structure-factor amplitudes calcu-

Table 1
Tetragonal hen-egg-white lysozyme *AGROVATA* processing statistics by resolution shell.

1° oscillation, 180 s exposure per frame.

D_{min} (Å)	R factor†	Average intensity	σ	I/σ	N_{meas}	N_{ref}
9.76	0.028	8527	619.1	13.8	259	59
7.09	0.015	10622	347.0	30.6	713	121
5.84	0.015	10808	270.9	39.9	958	158
5.08	0.015	11337	265.2	42.8	1162	184
4.56	0.014	14476	353.5	41.0	1279	201
4.17	0.016	17949	806.1	22.3	1372	215
3.87	0.017	17043	459.0	37.1	1605	247
3.62	0.019	14923	514.3	29.0	1670	256
3.42	0.020	12330	402.3	30.6	1850	274
3.24	0.022	9830	376.4	26.1	1995	290
3.09	0.022	8386	311.0	27.0	2064	300
2.96	0.024	6504	247.6	26.3	2192	313
2.85	0.026	4969	213.6	23.3	2305	334
2.75	0.027	4370	185.9	23.5	2338	331
2.65	0.025	4169	174.7	23.9	2492	355
2.57	0.027	3419	152.4	22.4	2584	364
2.49	0.032	2947	208.8	14.1	2614	367
2.42	0.037	2846	178.8	15.9	2519	378
2.36	0.040	2323	179.7	12.9	2239	379
2.30	0.044	2377	214.6	11.1	2104	391

† The R factors are the average $\Sigma(|I_i hkl - I_m hkl|/I_m hkl)$, where $I_i hkl$ is the ith measurement of the hkl reflection, $I_m hkl$ is the mean measured intensity for the hkl reflection; for reflections which have been measured more than once.

Table 2
Tetragonal hen-egg-white lysozyme *X-PLOR* R-factor statistics by resolution shell.

Only every third value is included to keep the table down to a reasonable size; the accumulative R values show that the missing values follow the same trend.

Minimum resolution (Å)	Maximum resolution (Å)	Number of reflections	R value†	Accumulative R value
8.03	15.00	105	0.2183	0.2183
5.27	5.77	121	0.1734	0.2127
4.40	4.62	117	0.1128	0.1763
3.91	4.05	115	0.1361	0.1583
3.59	3.69	115	0.1181	0.1516
3.35	3.43	120	0.1386	0.1473
3.17	3.23	110	0.1473	0.1472
3.02	3.07	106	0.1689	0.1477
2.89	2.93	119	0.1743	0.1493
2.79	2.82	116	0.1807	0.1518
2.70	2.72	110	0.2219	0.1548
2.61	2.64	108	0.1988	0.1567
2.54	2.56	116	0.1850	0.1584
2.48	2.50	108	0.2088	0.1610
2.42	2.44	109	0.2184	0.1633
2.36	2.38	116	0.2063	0.1654
2.32	2.33	111	0.1732	0.1663

† The R values are $\Sigma|F_o hkl - sF_c hkl|/\Sigma F_o hkl$, where $F_o hkl$ is the observed structure factor for the hkl reflection, $F_c hkl$ is the calculated structure factor from the model, and s is a scaling factor.

lated from the 1HEL model (Wilson, Malcolm & Matthews, 1992) were compared with the data. An R factor of 16.7% between 15 and 2.3 Å resolution was obtained without further refinement. The R factors and other statistics calculated by *X-PLOR* (Brünger, 1993) are shown for the different resolution shells in Table 2.

Off-axis data were also collected by translating the detector vertically. Similar processing statistics were obtained, showing that the detector may be successfully used in an off-axis geometry to collect higher resolution data. It should be noted that good symmetry-related peak R factors from data collected in an off-axis geometry are a good test of the flat-field correction.

The estimated r.m.s. positional errors of diffraction spots from these and previous data sets were ~30–40 μm in the X and Y directions, which is very comparable with data from the MarResearch scanner (X-ray Research GmbH, Segeberger Chaussee 34, 22850 Norderstedt, Germany). No problems were encountered with indexing.

3.4. *Practical resolution limits*

From experience of the detector performance, an estimate of the size of the unit cell which may be recorded and integrated to a given resolution may be made. This estimate is for a detector centred with respect to the direct beam. By going to off-axis geometries (by translation or rotation), higher resolution/larger unit-cell data may be collected, but the collection becomes less efficient because part of the resolution shells will not be recorded on a given image and larger total oscillation ranges are necessary.

The angular distance between spots recorded on an X-ray detector is given by the unit-cell axis divided by the wavelength (both in Å). The diffracted spot size and shape on the detector can be calculated by a knowledge of the sample size, mosaicity and the beam divergence conditions. Assuming a fixed pixel size of 120 μm and a square CCD chip of 1150 × 1150 pixels, the number of spots which may be fully resolved across the detector surface in 'symmetric' geometry can be calculated. The spot size on, for example, ESRF beamline BM-14 is typically 0.6 mm (5 pixels) given typical sample size, beam divergence, and using the full width at 1% maximum as a resolution criterion (Thompson *et al.*, 1996). It is advisable to measure at least as many pixels in the background as in the spot for reasonable peak integration. A closest peak spacing of 8 pixels gives 25 pixels in the peak and 39 pixels in the background. Under these conditions, a unit cell of longest dimension up to 200 Å can be resolved to 3 Å resolution.

The maximum scattering angle is presently limited to ~30° on the ESRF BM-14 beamline. This limitation is mainly due to the design of the diffractometer, which prevents the detector being moved very close to the sample. However, the convex form of the XRII detection surface means that as the sample is brought closer to the detector the angle with which high-angle reflections intersect the detector becomes increasingly small. Data collection with scattering angles of 45° and beyond may be viable, but the authors have no practical experience of this geometry.

4. Beamline ID-2 demonstration experiment

Following the success of the March 1995 test experiment, an opportunity to 'prove' the detector system and calibra-

Table 3
Summary of processing statistics from the ID-2 July experiment and BM-5 March experiment.

Sample	Collection details	Resolution (maximum) (Å)	$I/\sigma(I)$	*R*-merge factor (%)†	Crystallographic *R* factor (%)†
Tetragonal lysozyme	88° (30 s deg^{-1}) (BM-5)	2.3	23.0	2.1	16.7
HLA B8 complex 1	135° (10 s deg^{-1})	2.2	8.3	5.4	16.7
HLA B8 complex 2	180° (10 s deg^{-1})	2.1	5.1	8.6	18.3
HLA B8 complex 3	110° (10 s deg^{-1})	2.2	5.7	7.6	17.8
Phosphorylase kinase	135° (10 s deg^{-1})	2.2	22.6	5.1	21.3
Phosphorylase kinase	45° (15 s deg^{-1})	2.2	16.4	3.8	n.a.
Selenomethionine phosphorylase kinase derivative	90° [20 s (2 deg)$^{-1}$]	5.0	4.8	12.2	n.a.
SRP 9	60° (4 s deg^{-1})	3.0	5.5	9.2	n.a.

† The *R*-merge factors are defined in Table 1 and the crystallographic *R* factors are defined in Table 2.

tion methods under real experimental conditions came in July 1995 on ESRF beamline ID-2.

The same basic data-collection, calibration and processing strategy was used, but this time with a 1242 × 1152 pixel EEV CCD read-out with a 16-bit ADC, controlled by a Princeton Instruments Controller read into a Sun-10 workstation. A multitasking operating system such as Sun Solaris is more interesting than the DOS/Windows-based PC system for easier synchronization with the experiment and eventually for automatic correction and processing of the data. This different computing environment involved slight adaption of the data-collection methods previously developed.

The major difference between these experiments and those previously performed was the use of cryocooling on the samples. This introduced two additional potential problems: the magnetic goniostat head mount for the cryo-cooled samples, and the presence of the cryostream during calibration. Calibration tests with the magnetic cryomount in place showed no significant spatial changes owing to different rotations of the φ spindle. During calibration the cryostream was withdrawn slightly, and a piece of paper was used to divert the cold air stream to prevent any frosting on the fluorescent glass sample. If frosting were to occur, this could degrade the quality of the flat-field correction. With this simple precaution, the experiment was performed in the same manner as previous test experiments. Estimated peak centre positional errors produced by *DENZO* confirm that the magnetic cryomount did not noticeably degrade the quality of the spatial distortion correction.

Monochromatic data were collected using wavelengths between 0.75 and 0.87 Å, depending on the size of the sample unit cell or on the resolution required. None of the samples imposed strict requirements on wavelength, so rather than moving the detector, which would have required recalibration, the wavelength was altered. Oscillation ranges of 1° were used with exposure times varying from 4 to 20 s depending on the sample.

FIT2D was used to correct the data for spatial distortion and non-uniformity of response, *DENZO* was used to integrate the data, and *SCALEPACK* to scale the data and calculate statistics. All the data were corrected during the experiment, and initial integration and scaling was carried out for most of the data sets.

Full data sets were collected from six different samples, and a number of other samples were investigated in a period of ~30 h. About 4.5 Gbytes of raw data were collected, and a similar amount of corrected data were generated.

All data sets have been integrated and four have been analyzed through to electron-density maps. The remaining two data sets are higher resolution monochromatic data sets, depending on the solution of the structures from lower resolution data.

Brief details of the samples and the *R*-factor statistics obtained from the various data sets are shown in Table 3.

The major histocompatibility complex (MHC) molecule HLA B8 complexed with various peptides is being studied by Jones and co-workers from Oxford University Biophysics Department (Reid *et al.*, 1996). Recognition by T cell receptors of MHC Class I molecules complexed with peptides from pathogens serves to trigger the cellular immune response. Crystals of these complexes are of space group $P2_12_12_1$ with unit-cell dimensions a = 52, b = 81, c = 112 Å (slight variations occur with cryocooling) (Reid *et al.*, 1996). Although the complex crystals are well ordered, they are frequently small (0.1 × 0.05 × 0.2 mm) and necessitate high-intensity synchrotron radiation for high-resolution data. The rapid read-out of the CCD detector allowed high-resolution data sets for three complexes to be collected in less time than that required for collection of one such set using other types of on-line detector at a synchrotron. These three structures were solved by molecular replacement.

Noble and co-workers, also from Oxford University Biophysics Department, collected data from a truncated form of the γ-subunit of phosphorylase kinase (grown in the presence of the substrate analogue Mn^{2+}/AMPPNP). The structure of a truncated form of the γ-subunit of PhK has been reported at a resolution of 2.5 Å (Owen, Noble, Garman, Papageorgiou & Johnson, 1995) in space group $P2_12_12_1$ with cell dimensions a = 47.9, b = 69.1, c = 112.9 Å, $\alpha = \beta = \gamma = 90°$. Although most of the structure was well defined at this resolution, the conformation of one important loop, close to the presumed peptide substrate

binding site, remained unclear. This was due in part to the intrinsic flexibility of the loop and in part to problems with refinement against data of limited resolution. The experiment with the XRII/CCD allowed collection of a complete data set in one-fifth of the time used with the on-line imaging-plate system. The resulting data set showed good merging statistics to a resolution of 2.2 Å, and has been used to produce an improved model. In maps calculated with this model and the higher resolution data, a clear interpretation for the problem loop is suggested. A comparison of the electron-density map in the region of this loop for the 2.5 and 2.2 Å structures is shown in Fig. 3. The structure has been refined against the 2.2 Å data set to a 'free R factor' of 28.9% and a conventional R factor of 21.3%.

5. Discussion

5.1. *Data-collection times*

For the beamline ID-2 experiments, a typical 1° oscillation image took 30 s total collection time. Of this time, roughly 10 s were for the exposure, 10 s for the read-out and saving of the image to disk, and the remaining 10 s were due to a variety of delays necessary to ensure synchronization of the experiment control and the CCD data acquisition.

The 10 s exposure is caused by the small size and/or weak diffraction of the samples. These are the most scientifically interesting samples which are likely to be brought to third-generation sources. Whilst some small reduction in exposure length may come from even higher brilliance beamlines (since the experiment was performed, the ESRF normal running mode maximum electron current has been increased by 50%), several second exposure lengths are likely to remain.

The CCD read-out can be easily made much faster. The ESRF now has another Princeton camera with a 430 kHz read-out option, with almost 16 bits dynamic range (see §1). This allows read-out at full resolution in 3.3 s. Alternatively, a fast read-out camera has been built at the ESRF. This system has 1024 × 1024 pixels, 14 bits dynamic range, and can be read out at 5 MHz, allowing read-out in 0.2 s. (This system provides four parallel read-out channels and so can be read out in 0.05 s.) The saving of images to disk will typically take 1–2 s, but this time can be avoided by using double-buffering in the computer memory and making the disk writing operation simultaneous with the exposure and subsequent read-out operations.

The 10 s used for synchronization can be very largely reduced by streamlining the data-collection protocol, and by using hardware synchronization. (For the beamline ID-2 experiment, hardware synchronization was not available and relatively long delays were needed owing to the lack of real-time support of the Unix operating system.) Some overheads will always be necessary owing to the need to ensure that the spindle axis is at full rotation speed when the X-ray shutter opens, but with careful design it should be possible to reduce the overheads to ~1 s.

With slightly more brilliant X-ray sources, it is conceivable to collect such oscillation data at an image every 10 s, for 1° oscillations. A 90° monochromatic data set would be completed in 15 min.

5.2. *Benefits for data quality*

Crystals which produce relatively high backgrounds owing to solvent and other diffuse scattering are important limitations to the signal-to-noise ratio. Using smaller

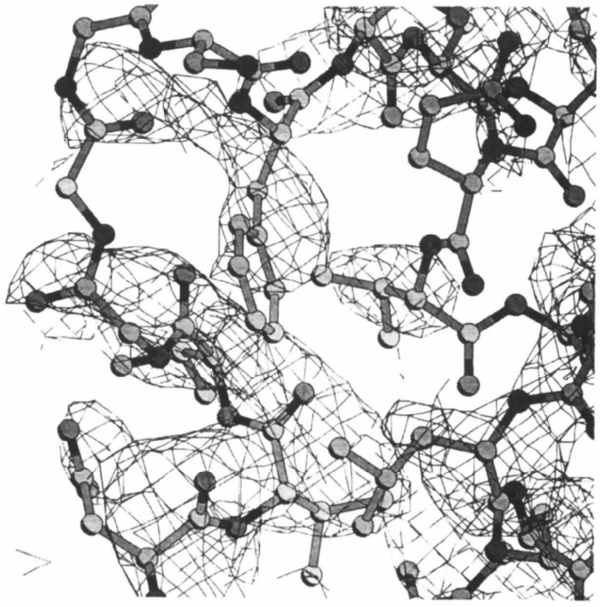

(*a*)

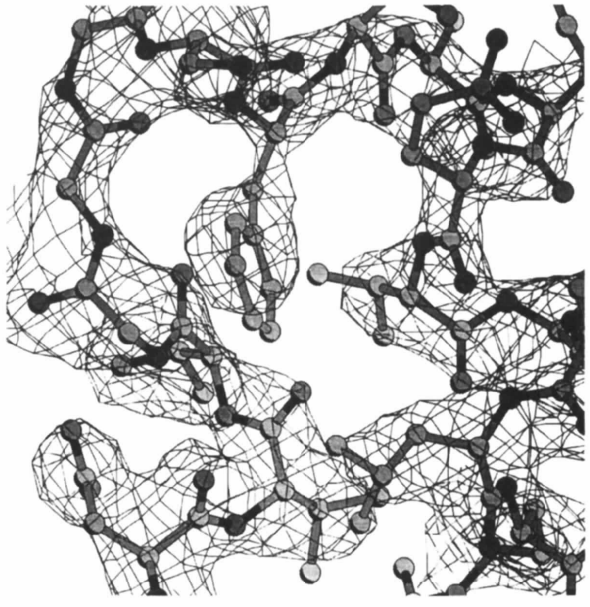

(*b*)

Figure 3
Electron density maps ($2F_o - F_c$) calculated from (*a*) 2.5 Å resolution data set collected with a MarResearch imaging-plate system, and (*b*) 2.2 Å resolution data set collected with the XRII/CCD. Both maps are contoured at a level of 0.8 times the r.m.s. electron density of the map. The refined 2.2 Å resolution model is superposed.

oscillation ranges is one potential method for reducing this background noise since typical crystal rocking widths are smaller than the normally used 1° oscillation ranges. Fourme, Bahri, Kahn & Rosshard (1991) have reported the advantage of using small-oscillation-range data collection by comparing data sets collected in 0.05° frames and 1° frames, using crystals from the same batch. The $R_{\rm merge}$ factor for the 1° data set was 4.6% and for the 0.05° data set was 2.8% (note that the difference in data quality is also, to some extent, due to the photon-counting nature of the multiwire proportional counter which was used to collect the 0.05° data set compared with the integrating imaging-plate detector used for the 1° data set).

Fast read-out detectors make smaller oscillation ranges a practical possibility since the data-collection time is mainly dependent on the exposure time per degree, so the total time is only slightly increased by taking more smaller oscillation-range images. As an example of the benefit from smaller oscillation ranges, a recent sample was collected with the XRII/CCD on beamline BM-14 in both 1 and 0.5° frames. Different crystals from the same batch and of similar size were used. The $R_{\rm merge}$ factor from the 1° data set was 4.8%, compared with 3.4% from the 0.5° data set (Pauptit, 1996). Note that this difference was observed with a cryocooled crystal; the improvement in small oscillation-range images may be smaller for a high mosaic crystal than for a non-mosaic crystal, but in many cases will still be far from negligible.

The combination of very high brilliance 'third-generation' synchrotron radiation X-ray sources and fast read-out detectors provides the opportunity to collect data much more quickly than has previously been possible. This is likely to open new possibilities for macromolecular crystallography. Henderson (1990, 1995) and Nave (1995) have discussed the radiation damage of protein crystals in an X-ray beam at cryocooled temperatures. The data quality from certain crystals which cannot be frozen may be much improved, and it is possible that in cases where significant time-dependent radiation damage can still occur even at 100 K, the fast read-out of the detector could be an important factor in collecting data to the highest possible resolution. There is, to date, only anecdotal evidence to support this suggestion.

5.3. *Interpretation of data quality from test samples*

The interpretation of data quality from test crystals deserves careful consideration. For obvious reasons, strongly diffracting samples such as lysozyme are usually used as test samples. Problems with data collection or calibration should be evident given the intrinsic high data quality which should be obtained. However, such results are not a good indication of the true merit of the detector system for the real scientific samples of interest. The scientifically interesting samples are generally much more weakly diffracting so the ratio of Bragg peak intensities to diffuse background is much smaller. Different detector characteristics may be of importance in obtaining the best data quality from 'real' samples rather than those deduced from test experiments.

For future testing of the effect of using narrower oscillation ranges we plan to develop artificially high background test 'samples', *e.g.* small crystals with deliberately much larger beam sizes.

5.4. *Data quantities*

Fast read-out on-line detectors can produce relatively large quantities of data. The ID-2 experiment produced 4.5 Gbytes of raw data in 30 h. Faster read-out in itself will not produce much more data, as already the 'down time' owing to refilling, crystal mounting and screening for good crystals takes more time than the data collection from 'good' crystals.

If smaller oscillation ranges or larger detectors are used, data quantity will increase. If, for example, 0.25° oscillations are used instead of 1° oscillations, the daily data production could be ~20 Gbytes.

Additionally, MAD data sets could be three or even five times larger than equivalent single-wavelength ones, and with cryocooling a single crystal may be used to collect a complete data set in 1 h.

These quantities of data may seem large, but cheap and readily available modern computing devices can easily handle this as long as a locally based ('distributed') computing strategy is followed. 9 Gbyte disks are now common and cheap. A full 180° monochromatic data set taken in 0.25° oscillations would be ~2 Gbytes of raw data, but still fits onto a DAT tape. A day's data collection would fit onto ten or less such tapes. It will probably be necessary to provide at least two DAT tape drives per beamline end-station as the writing of the tapes is slow.

There is a highly understandable desire to be able to transfer raw data between institutes by international computer communication networks, but unless there is a very major upgrading of such networks this will remain an impractical wish for the foreseeable future. For raw data transfer, recording media (magnetic or optomagnetic at present) will doubtlessly remain the only viable transfer mechanism for such data quantities. Faster and larger capacity storage media will hopefully become more 'standardized' and widespread in the near future. DLT tapes can presently store up to 70 Gbytes and aim to store 100 Gbytes on a single cassette. The limiting factor in the uptake of such technology is its widespread acceptance and availability. It is of little use to write data onto such tapes if a tape reader is not available at the 'receiving' institute. At present, DAT technology is sufficiently cheap that DAT tape drives are reasonably common even in small laboratories. Another interesting transfer mechanism is portable SCSI (small computer systems interface) disks.

The above estimates have ignored the possibility of data compression. Standard computer compression utilities offer very little gain, but compression methods which utilize the fact that the value of one pixel tends to be similar to the value of the neighbouring pixels can achieve compression

ratios of 2.5–3 on typical diffraction images, without any loss of information.

An alternative solution to the problem of data transfer is to perform data reduction at the source and only transfer processed data such as *hkl* integrated intensities. This implies the existence of sufficiently powerful 'on-line' systems. These must be powerful, both in terms of computing power, so that they can keep pace with the detectors, and in the sense of achieving good integration with little or no user intervention. 'On-line' data-reduction systems would also be important in monitoring data quality whilst experiments progressed. Systems of this type are presently under development (Otwinoski & Minor, 1995). Such an approach also requires that it is accepted by the scientists, *i.e.* they accept the resulting data quality and only return with the processed results.

6. Conclusions

The XRII/CCD detector system has been demonstrated to produce high-quality macromolecular crystallography data and allows much faster data collection than the presently used on-line imaging-plate systems. Data collection has been tested successfully under real experimental conditions, including the complications caused by cryocooling. The faster data-collection time results both in higher redundancy data sets and more samples being studied. This is important given the high cost and limited accessibility of synchrotron radiation sources. The faster data collection may be important in obtaining higher quality/higher resolution data for certain samples.

Calibration techniques have been developed which may be of great benefit in obtaining high-quality data from other imaging detectors. In particular, the use of fluorescence from doped dilithium tetraborate glasses is a novel technique with the potential to improve quantitative results from two-dimensional detectors.

A beryllium-entrance-window XRII is now being used routinely as the main detector on the ESRF multiple anomalous diffraction (MAD) beamline (BM-14) (Thompson *et al.*, 1996). Work has continued further improving calibration techniques and data quality, and challenging MAD experiments and small-molecule crystallography experiments (Müller *et al.*, 1997) have been successfully performed. The results from MAD experiments are very encouraging: high-quality anomalous and dispersive Patterson maps have been obtained from a number of samples (Haedener *et al.*, 1997), and recently the structure of maclura pommifera aglutinin (MPA) was solved to a resolution of 2.9 Å using MAD phasing and a Pb derivative (Lee *et al.*, 1997).

These types of experiments require very accurate integrated-intensity information. Optically thicker fluorescence samples have been used to produce yet smoother and more symmetric flood-field emissions. The spatial distortion calibration now accounts for 'mask vignetting', which is the partial shadowing of the calibration grid holes for off-axis sources owing to the thickness of the grid. A more accurate rebinning algorithm, which calculates the overlap areas of distorted quadrilateral pixels, has been implemented.

Easy use of detector systems is an important issue for a user facility. The calibration and correction procedures used are presently time consuming. Eliminating the need for users to perform calibration measurements and making the correction procedures automatic is highly desirable and is being investigated. If the geometrical parallax can be separated from the other distortion effects then it should be possible to avoid recalibration for different experiment geometries. Calibration would then only be necessary occasionally.

The authors would like to thank for their contribution and support the visiting experimentalists from Oxford University: K. Smith, M. Noble, M. O'Reilly, E. Y. Jones, S. W. Reid; the staff of ESRF beamline ID-2, especially A. Åberg, who managed the computing environment; Princeton Instruments for the loan of the CCD controller to Sun workstation data link; Z. Otwinowski and W. Minor (*DENZO/SCALEPACK*) and the CCP4 staff and contributors; J. Klora and the ESRF Instrument Control group for motor control and computing support for data acquisition; A. Freund and ESRF BM-5 staff for use of the beamline and related facilities; J. Baruchel and members of the ESRF Topography group for use of their equipment and help with running it, with special thanks to R. Barrett; the ESRF Diffraction Group for loan of the detector system; W. C. A. Pulford for help with PC hardware and software; the EMBL Grenoble for loan of the Arndt–Wonacott camera and other general support; and the ESRF directorate for support of this work.

References

Brünger, A. T. (1993). *X-PLOR. A System for Crystallography and NMR*. Version 3.1. Yale University Press.

Collaborative Computational Project, Number 4 (1994). *Acta Cryst.* D**50**, 760–763.

Deckman, H. W. & Gruner, S. M. (1986). *Nucl. Instrum. Methods*, A**246**, 527–533.

Fanchon, E., Ferrer, J.-L., Kahn, R., Berthet, C. & Roth, M. (1995). *ESRF Newsl.* **24**, 6–7.

Fourme, R., Bahri, A., Kahn, R. & Rosshard, R. (1991). *Proceedings of the European Workshop on X-ray Detectors for Synchrotron Radiation Sources*, Aussois, edited by A. H. Walenta, pp. 16–25. University of Siegen, Germany.

Foust, S. (1995). Internal Report EXP/SF/1995/01. ESRF, Grenoble, France.

Haedener, A., Niemann, A., Helliwell, J. R., Cassetta, A., Thompson, A. W. & Hammersley, A. P. (1997). *Acta Cryst.* D. In preparation.

Hammersley, A. P. (1995) *FIT2D* V5.18 *Reference Manual* V1.6. Internal Report EXP/AH/95-01. ESRF, Grenoble, France.

Hammersley, A. P., Svensson, S. O. & Thompson, A. (1994). *Nucl. Instrum. Methods*, A**346**, 312–321.

Hammersley, A. P., Svensson, S. O., Thompson, A., Graafsma, H., Kvick, Å. & Moy, J.-P. (1995). *Rev. Sci. Instrum.* **66**, 2729–2733.
Henderson, R. (1990). *Proc. R. Soc. London Ser. B*, **241**, 6–8.
Henderson, R. (1995). *Q. Rev. Biophys.* **28**, 171–193.
Labiche, J.-C., Segura-Puchades, J., van Brussel, D. & Moy, J.-P. (1996). *ESRF Newsl.* **25**, 41–43.
Lee, X., Zhang, Z., Hoa, T., Xu, L., Biesterfeld, J., Young, M. & Johnston, R. (1997). In preparation.
Moy, J.-P. (1994). *Nucl. Instrum. Methods*, A**348**, 641–644.
Moy, J.-P., Hammersley, A. P., Svensson, S. O., Thompson, A., Brown, K., Claustre, L., Gonzalez, A. & McSweeney, S. (1996). *J. Synchrotron Rad.* **3**, 1–5.
Müller, H., Svensson, S. O., Xenikos, D. G., Lorenzen, M., Fitch, A. & Kvick, Å. (1997). In preparation.
Naday, I., Ross, S., Kanyo, M., Westbrook, E. M. & Westbrook, M. L. (1994). *Nucl. Instrum. Methods*, A**347**, 534–538.
Naday, I., Ross, S., Kanyo, M., Westbrook, M. L., Westbrook, E. M., Phillips, W. C., Stanton, M. S. & Nara, D. O. (1995). *SPIE J.* **2415**, 236–249.
Nave, C. (1995). *Radiat. Phys. Chem.* **45**, 483–490.
Otwinowski, Z. (1993). *Proceedings of the CCP4 Study Weekend: Data Collection and Processing*, 29–30 January 1993, compiled by L. Sawyer, N. Isaacs & S. Bailey, pp. 56–62. SERC Daresbury Laboratory, Warrington, UK.
Otwinowski, Z. & Minor, W. (1995). Personal communication.
Owen, D. J., Noble, M. E. M., Garman, E. F., Papageorgiou, A. C. & Johnson, L. N. (1995). *Structure*, **3**, 467–482.
Pauptit, R. (1996). Personal communication.
Reid, S. W., Smith, K. J., Jacobsen, B., O'Callaghan, C., Reyburn, H., Harlos, K., Stuart, D. I., McMichael, A., Bell, J. & Jones, E. Y. (1996). *FEBS Lett.* **383** 119–123.
Stanton, M., Philips, W. C., Li, Y. & Kalata, K. (1992). *J. Appl. Cryst.* **25**, 549–558.
Tate, M. W., Eikenberry, E. F., Barna, S. L., Wall, M. E., Lowrance, J. L. & Gruner, S. M. (1995). *J. Appl. Cryst.* **28**, 196–205.
Thiel, D. J., Walter, R. L., Ealick, S. E., Bilderback, D. H., Tate, M. W., Gruner, S. M. & Eikenberry, E. F. (1995). *Rev. Sci. Instrum.* **66**, 1477–1479.
Thomas, D. J. (1989). *Proc. R. Soc. London Ser. A*, **425**, 129–167.
Thomas, D. J. (1990). *Proc. R. Soc. London Ser. A*, **428**, 181–214.
Thompson, A. W., Biou, V., Claustre, L., Felisaz, F., Gonzalez, A., Helliwell, J. R., Smith, J. L., Hammersley, A. P. & Thorander, P. (1996). *Acta Cryst.* A**52**, C-20.
Walter, R. L., Thiel, D. J., Barna, S. L., Tate, M. W., Wall, M. E., Eikenberry, E. F., Gruner, S. M. & Ealick, S. E. (1995). *Structure*, **3**, 835–844.
Wilson, K. P., Malcolm, B. A. & Matthews, B. W. (1992). *J. Biol. Chem.* **267**, 10842–10849.